

UV Colors and Extinctions of HII Regions in the Whirlpool Galaxy (M51)

Jesse K. Hill^{1,5}, William H. Waller^{1,5}, Robert H. Cornett^{1,5}, Ralph C. Bohlin²

K.-P. Cheng⁷, Susan G. Neff⁵, Robert W. O'Connell³, Morton S. Roberts⁴

Andrew M. Smith⁵, P. M. N. Hintzen^{5,6}, Eric P. Smith⁵

Theodore P. Stecher⁵

Received _____; accepted _____

¹Hughes STX, 4400 Forbes Blvd, Lanham, MD 20706

²Space Telescope Science Institute, Homewood Campus, Baltimore, MD 21218

³University of Virginia, P. O. Box 3818, Charlottesville, VA 22903

⁴National Radio Astronomy Observatory, Edgemont Rd., Charlottesville, VA 22903

⁵Laboratory for Astronomy and Solar physics, NASA/GSFC, Greenbelt, MD 20771

⁶California State University, Dept. of Phys. & Astron., Long Beach CA 90840

⁷California State University, Dept. of Phys., Fullerton CA 92634

ABSTRACT

Far-UV (wavelength 1520 Å), U, H α , and R images of the interacting Sbc spiral galaxy M51 were obtained by the Ultraviolet Imaging Telescope (UIT) during the *Astro-2* Spacelab mission of 1995 March and at Mt. Laguna Observatory. The $\mu_{152} - \mu_U$ radial gradient of over a magnitude, becoming bluer with increasing radius, is attributed primarily to a corresponding radial extinction gradient. Magnitudes in both UV bands and H α fluxes are reported for 28 H II regions. Optical extinctions for the 28 corresponding UV sources are computed from the measured $m_{152} - U$ colors by fitting to the optical extinctions of Nakai & Kuno (1995). The normalized far-UV extinction $A_{152}/E(B - V)$ increases with increasing galactocentric distance or decreasing metallicity, from 5.99 to 6.54, compared with the Galactic value 8.33. The best-fit $m_{152} - U$ color for no extinction, -3.07 , is the color of a model solar metallicity starburst of age ~ 2.5 Myr with IMF slope -1.0 . HII regions show decreasing observed H α fluxes with decreasing radius, relative to the H α fluxes predicted from the observed f_{152} for age 2.5 Myr, after the H α and f_{152} are corrected for extinction. We attribute the increasing fraction of “missing” H α flux with decreasing radius to increasing extinction in the Lyman continuum. The increasing extinction-corrected far-UV flux of the H II regions with decreasing distance to the nucleus is probably a result of the corresponding increasing column density of the interstellar gas resulting in larger mass OB associations. The estimated dust-absorbed Lyman continuum flux is ~ 0.6 times the far-infrared energy flux of M51 observed by IRAS.

Subject headings: galaxies: individual: M51, HII Regions, ultraviolet:
general

1. Introduction

Because of its proximity, almost face-on orientation, and prominent spiral structure, the interacting Sbc galaxy M51 has been a favorite target of observational astronomers for many years. The Ultraviolet Imaging Telescope image of M51 reported here, obtained with ~ 3 arcsec resolution, represents a 5-fold increase in resolution compared to prior UV imaging (Bohlin et al. 1990a; Bersier et al. 1994). The image was obtained during the Astro-2 spacelab mission of 1995 March. Ultraviolet images of spiral galaxies are dominated by the OB/H II complexes in the spiral arms (Hill, Bohlin & Stecher 1984; Bohlin et al. 1990a, 1990b; Hill et al. 1992). Complementary CCD images in the U, H α , and R bands were obtained at Mt. Laguna Observatory to better investigate the star-forming complexes. A log of the observations used in this investigation is given in Table 1.

UIT is a 38 cm Ritchey-Chrétien telescope, which images a 40' diameter field to the cathode of a two-stage magnetically focussed image intensifier, coupled by fiber optics to II-aO film. The intensifier has a UV-sensitive, solar-blind CsI photocathode. (The intensifier for the near-UV camera, which functioned well during the 1990 Astro-1 mission, was apparently damaged during the Astro-2 launch, so near-UV data were obtained from the ground in the U band.) The UIT instrument, the available bandpasses, and the reduction of the digitized film images to arrays of flux-calibrated integer pixels are discussed by Stecher et al. (1992). The bandpass used in this investigation is termed B1, with centroid 1520 Å and width 354 Å. Fluxes f measured in this UIT band are converted to magnitudes m_{152} by the relation $m_{152} = -2.5 \times \log f - 21.10$. The longest B1 exposure obtained, and the one used in this investigation, is of duration 1100.5 s. A north-up, east-left version of the image was corrected for image distortion using the method of Greason et al. (1994) and used for subsequent analysis.

A UIT precursor aboard a sounding-rocket imaged M51 at wavelength 2250 Å, with 15

arcsec resolution (Bohlin et al. 1990a). The most prominent features in M51 at 2250 Å are a region surrounding the nucleus, of size ~ 1 arcmin and the group of bright H II regions about 2 arcmin NE from the nucleus. The interacting companion NGC 5195 is much less prominent in the near-UV than at optical wavelengths. The nuclear region shows a complex structure, with evidence for star formation and possibly for an Inner Lindblad Resonance at radius $\sim 10 - 15$ arcsec. In combination with a digitized photographic image in the U band, evidence was found for a variation in $m_{225} - U$ colors of bright H II regions of about 1 magnitude (here, m_{225} is the magnitude in the sounding rocket band).

A UV image of M51 at wavelength 2000 Å, also with 15 arcsec resolution, was obtained by Bersier et al. (1994) with a balloon-borne telescope. Bersier et al. found that the UV emission in the spiral arms usually peaks about 7–11 arcsec in the direction of galactic rotation from the H α emission. They estimated star formation rates and star formation efficiencies.

CCD images of M51 were obtained in the Johnson U band, the Kron-Cousins R band, and at H α with the Mt. Laguna 1.0 m using an interference filter of bandwidth 61Å. Figures 1a–1c (Plates XX-XX) show the UIT far-UV image, the U image, and the H α image, after subtraction of the red continuum according to the formulations in Waller (1990). The companion galaxy NGC 5195, visible on the U band image, is not detectable on the UIT far-UV image. The sounding rocket image appears as Figure 1b in Bohlin et al. (1990a). We present and discuss multiband photometry of 28 M51 UV sources, and surface photometry in the far-UV and U band images. The 28 UV sources investigated are circled on Figures 1a–1c.

2. The UV Color profile and Source Photometry

From a Fourier analysis of their UV image, Bersier et al. (1994) determined the position angle and inclination of M51 to be 26 degrees and 42 degrees, respectively, consistent with previous estimates. We adopt their position angle and inclination to construct equivalent face-on azimuthally averaged radial profiles in the UIT B1 band and the ground-based U band. The UV profiles are similar to the profile of Bersier et al. (1994) and the profile of Bohlin et al. (1990a). From the B1 and U band profiles the $\mu_{152} - \mu_U$ color profile is constructed and plotted in Figure 2. A UV color gradient of about 2 magnitudes is found from the nucleus to the outermost measured UV sources, at radius 11 kpc.

We identify 28 spiral arm sources on the UIT image with average separation 2.6 arcsec from the corresponding H II region on the H α image, coincident within the estimated accuracy of the distortion correction applied to the UIT images (Greason et al. 1994). Aperture photometry is performed of these sources on the UV and H α images with apertures of radius 8 arcsec (370 pc for distance 9.6 Mpc). The sky value is determined as the mode of pixels within annuli with inner and outer radii 11 and 22 arcsec. Aperture photometry is performed using IDL implementations of DAOPHOT software (Stetson 1987). No aperture correction is employed in the UIT image photometry because any extended emission beyond the boundary of the 8.0 arcsec aperture appears to be associated with extended, diffuse spiral arm emission, rather than the source itself. The H α aperture correction for the nearly-isolated H II region Rand 454, is only about 25%. Hence, we apply no aperture corrections to the H α fluxes either, because the corrections are small, and also because the sources do not have identical profiles.

IUE spectra of isolated stars from several fields observed by UIT are utilized in determining the UIT calibration, thought to be accurate to about 15% relative to *IUE*. UIT instrumental fluxes used in determining the calibration are from apertures large enough to

contain all the stellar flux. Calibration of the U band photometry, with uncertainty about 5%, is based on the photoelectric photometry of Schweizer (1976).

Subtraction of the red continuum from the $H\alpha$ band image is accomplished by scaling count rates of stars in the R image to equal their counterparts in the $H\alpha$ image (Waller 1990). The effect of line emission in the R-band image is estimated and removed using the filter curves for the two bands. The contribution of [NII] ($\lambda\lambda 6548, 6584$) line emission to the total $H\alpha$ + [NII] line flux is estimated to be 35% in emission (McCall et al 1985) and 28 % through the $H\alpha$ filter. McCall et al. (1985) have determined that the ratio [NII]/ $H\alpha$ is independent of excitation over a range -0.35 to -0.56 in $\log ([OII] + [OIII])/H\beta$. The quoted $H\alpha$ fluxes have been corrected accordingly. Absolute calibration of the $H\alpha$ and R images uses CCD images of the spectrophotometric standard star BD +08 2015 taken on the same photometric night with the same instrument. The resulting $H\alpha$ photometry of the H II region Rand 454 agrees with that of Rand (1992) to within 8%.

UV magnitudes and $H\alpha$ fluxes for the 28 sources are given in Table 2. Table 2 contains the source index number (col. 1), the H II region number from Rand (1992) (col. 2), the distance in arcsec east of the nucleus (col. 3), the distance in arcsec north of the nucleus (col. 4), the far-UV magnitude m_{152} (col. 5), the estimated error in the far-UV magnitude (col. 6), the U magnitude (col. 7), the estimated error in the U magnitude (col. 8), the $H\alpha$ flux (col. 9), the estimated fractional error in the $H\alpha$ flux (col. 10), and the A_V computed from the UV color (col. 11). Figure 2, which plots the large-scale radial variation in the $\mu_{152} - \mu_U$ color, also plots as solid circles the $m_{152} - U$ colors of the 28 UV sources. The colors of the sources are $\sim 0.5 - 1.0$ mag bluer than the large-scale UV color at the same radius, in nearly all cases. The UV CMD for the H II regions of M51 is similar to the UV CMD for the M81 HII regions (Hill et al. 1995), except that for M81 the UIT near-UV magnitudes m_{249} were used, rather than ground-based U. The brightest of the 28 sources in

the far-UV band has luminosity about 800 times the far-UV luminosity of the Orion Nebula (Bohlin et al. 1982), while the faintest has a far-UV luminosity ~ 80 times that of Orion.

3. Extinctions and Ages of HII Regions

Evolving star cluster spectra are modeled using the evolutionary stellar models of Schaller et al. (1992), together with the model atmospheres of Kurucz (1992) for IMF slopes -1.0 , -1.5 , and -2.0 , assuming solar metallicity. For each of these evolving models, $m_{152} - U$ colors are determined as a function of age. For an IMF slope equal to -1.0 , close to the slope -1.08 found by Hill et al. (1994) for the OB associations near 30 Dor, the UV color begins at ~ -3.2 at age zero, and evolves to $\sim -2.6 \pm 0.16$ for ages $3 - 15$ Myr. Steady-state star formation models predict $m_{152} - U$ colors -2.47 , -2.21 , and -1.92 for the three IMF slopes. Steady-state models with twice solar metal abundances give UV colors redder by ~ 0.10 mag for the three IMF slopes. The relatively modest change in predicted UV color for a factor two increase in metallicity suggests that the primary cause of the observed color gradient in M51 is a radial extinction gradient.

Nakai & Kuno (1995) revised the A_V for the H II regions observed by van der Hulst et al. (1988), taking into account the variation in H II region gas temperature caused by the effect of the metallicity gradient on the abundance of coolants. A linear relation is fit between the revised A_V of Nakai & Kuno and the $m_{152} - U$ colors measured here, for the 14 H II regions in common between the two lists. The fit relation between the A_V of Nakai & Kuno (1995) and the UV colors is then used to estimate A_V for all 28 H II regions. We estimate the metallicities of the H II regions from the galactocentric distance, assuming that the H II region Rand 454 has solar metallicity and that the metallicity variation with increasing distance is -0.14 dex/arcmin (Villa-Costas & Edmunds 1992).

The UV spectrum over the wavelength interval 400 to 4000 Å is computed for IMF slope -1.0 (Hill et al. 1994), age 2.5 Myr, and metallicities equal to the solar metallicity and twice the solar metallicity, using the evolutionary models of Schaller et al. (1992). For twice solar metallicity, the predicted ratio of Lyman continuum flux to the flux at 1500 Å is only half that predicted for solar metallicity. The spectra of the innermost H II regions, whose metallicities are estimated at ~ 4 times solar, are extrapolated from the 2 times solar metallicity model. For them, the predicted ratio of Lyman continuum flux to the flux at 1500 Å is only 0.3 times that predicted for solar metallicity. UV colors $m_{152} - U$ are computed from these model spectra, and used to determine the variation of the unreddened UV color with radius, allowing computation of the UV color excess $E(m_{152} - U)$ for each of the H II regions. The ratio of the UV color excess to $E(B - V)$ is then used to derive far-UV extinctions, by interpolating the normalized far-UV extinction over the normalized UV color excess between the 30 Dor nebular extinction curve (Fitzpatrick & Savage 1984), and the Orion extinction curve (Bohlin & Savage 1981). We derive normalized far-UV extinctions $A_{152}/E(B - V)$ for the H II regions which vary from 5.99 to 6.54, with average value 6.26. These normalized far-UV extinctions are plotted versus metallicity relative to solar in Figure 3. The best-fit $m_{152} - U$ color for zero extinction is -3.07 , the color of an evolving solar metallicity starburst of age ~ 2.5 Myr, approximately the average age obtained by Hill et al. (1995) for the M81 H II regions.

The optical extinctions A_V estimated from the UV colors for the 28 HII regions are given in Table 2, col. 11. Ages for these sources are estimated to be ~ 2.5 Myr. Because these 28 H α sources are closely coincident with the corresponding far-UV sources, we can estimate the fraction of the Lyman continuum photons which are absorbed by HI atoms rather than by dust grains, as the ratio of the observed H α flux (corrected for the extinction estimated from $m_{152} - U$) to the H α flux expected from the extinction-corrected m_{152} , the evolving starburst model with IMF slope equal to -1.0 , and the assumption that the age is

2.5 Myr, and taking into account the variation of metallicity with radius.

We define an effective Lyman continuum extinction as $A_{Ly,eff} = 2.5 \times \log(f_{H\alpha,UV}/f_{H\alpha})$, where $f_{H\alpha,UV}$ is the H α flux predicted from the extinction corrected UV flux and the assumed age 2.5 Myr, and $f_{H\alpha}$ is the extinction corrected H α flux. Figure 4 plots the effective Lyman continuum extinction vs. E(B-V) computed from the estimated V-band extinction. The plot shows that the two measures of extinction are strongly correlated. The ratio $A_{Ly,eff}/E(B - V)$ is approximately equal to the normalized extinction in M51 at a typical Lyman continuum wavelength, times the fraction of the E(B-V) which takes place inside the H II region. If the normalized extinction at Lyman continuum wavelengths in M51 is approximately equal to 19.0, the value obtained by Clayton et al. (1996) for two lines of sight in the LMC, then for the 28 H II regions investigated here, the fraction of the optical extinction which takes place inside the H II region averages 0.15, and ranges from 0.07 to 0.23.

We define “missing” H α flux as the difference between the H α flux predicted by the corrected UIT flux and the corrected H α flux. The estimated ratio of the “missing” Lyman continuum energy flux (equal in photon flux to \sim twice the “missing” H α flux), to the total observed IRAS energy flux is 0.60.

The extinction-corrected far-UV magnitudes of the UV sources become brighter with decreasing distance from the nucleus. The masses of the OB associations exciting the H II regions are expected to be proportional to the corrected far-UV fluxes. The interstellar gas column densities exhibit a similar trend (Nakai & Kuno 1995). The CO azimuthal profiles of Kuno et al. (1995) show larger peak fluxes above background in the integrated intensity for decreasing radii, which is consistent with an increase in the masses of the OB associations exciting the H II regions with decreasing galactocentric radius.

4. Acknowledgements

We gratefully acknowledge the contributions made by the many NASA personnel involved in the *Astro-2* mission. We also thank IPAC personnel for providing the HIRES IRAS images of M51 used in this investigation.

Funding for the UIT project has been through the Spacelab Office at NASA headquarters under Project number 440-51. RWO gratefully acknowledges NASA support of portions of this research through grants NAG5-700 and NAGW-2596 to the University of Virginia.

Table 1. Log of Observations of M51

Observatory	Telescope	band	wavelength (\AA)	bandwidth (\AA)	exposure time (s)
<i>Astro-2</i>	UIT	B1	1520	354	1100.5
Mt. Laguna	1m	U	3650	700	1200.0
Mt. Laguna	1m	H α	6573	61	600.0
Mt. Laguna	1m	R	6500	1500.0	1500.0

Table 2. HII Regions

Ind	Rand	X	Y	m_{152}	err	U	err	$f_{H\alpha} \times 10^{14}$	frac. err	A_V
1	190	158.1	68.5	15.08	0.08	16.46	0.08	3.07	0.93	2.41
2	173	144.6	-7.7	14.76	0.04	16.38	0.06	7.61	0.37	2.06
3	218	118.2	230.0	15.30	0.06	17.33	0.12	8.78	0.32	1.48
4	219	112.5	240.0	15.47	0.07	17.97	0.22	7.35	0.38	0.81
5	147	106.6	-108.8	14.64	0.05	16.05	0.05	17.69	0.16	2.36
6	321	99.1	142.5	14.85	0.08	16.45	0.06	8.37	0.34	2.10
7	146	97.8	-113.2	14.63	0.04	15.97	0.05	25.60	0.11	2.46
8	275	93.6	10.3	15.25	0.08	16.09	0.06	6.00	0.47	3.18
9	307	87.8	67.8	14.03	0.04	15.45	0.04	14.68	0.19	2.35
10	309	86.2	82.0	13.75	0.03	15.22	0.03	19.73	0.14	2.29
11	270	84.2	-4.1	14.59	0.05	15.62	0.04	9.78	0.29	2.90
12	142	82.5	-133.6	16.24	0.20	17.49	0.15	7.49	0.38	2.60
13	320	72.0	134.3	13.94	0.05	15.40	0.06	28.05	0.10	2.30
14	323	59.6	145.4	14.59	0.07	15.66	0.05	13.59	0.21	2.85
15	24	34.5	52.4	15.35	0.08	15.99	0.05	5.23	0.54	3.46
16	9	34.3	12.0	14.10	0.04	15.08	0.03	5.20	0.55	2.98
17	332	31.8	136.9	14.72	0.06	16.08	0.06	15.93	0.17	2.44
18	13	18.3	22.6	14.23	0.06	14.94	0.03	5.43	0.54	3.37
19	32	-6.0	59.6	15.32	0.07	15.96	0.05	21.20	0.13	3.47
20	96	-22.0	-145.7	15.07	0.06	16.36	0.06	4.28	0.66	2.54

Table 2—Continued

Ind	Rand	X	Y	m_{152}	err	U	err	$f_{H\alpha} \times 10^{14}$	frac. err	A_V
21	401	-54.5	111.1	13.93	0.02	15.34	0.03	11.76	0.24	2.36
22	80	-57.7	-123.7	14.41	0.04	15.77	0.04	6.41	0.44	2.43
23	45	-62.7	46.6	15.25	0.06	16.22	0.06	7.12	0.40	2.99
24	403	-66.2	116.7	14.58	0.05	15.93	0.05	7.96	0.35	2.45
25	79	-78.8	-106.5	13.74	0.02	14.95	0.03	30.29	0.09	2.65
26	...	-87.9	-79.9	14.15	0.03	15.28	0.04	36.52	0.07	2.77
27	61	-98.0	-9.4	14.17	0.03	15.45	0.04	6.34	0.45	2.55
28	455	-137.8	-182.4	16.09	0.14	17.36	0.11	14.76	0.19	2.58

REFERENCES

- Bersier, D., Blecha, A., Golay, M., & Martinet, L. 1994, *A&A*, 286, 37
- Bessell, M. S. 1979, *PASP*, 91, 589
- Bohlin, R. C, Cornett, R. C., Hill, J. K., O'Connell, R. W., & Stecher, T. P. , 1990a, *ApJ*, 352, 55
- Bohlin, R. C., Hill, J. K., Stecher, T. P., & Witt A. N., 1982, *ApJ*, 255, 87
- Bohlin, R. C., Cornett, R. H., Hill, J. K., & Stecher, T. P., 1990b, *ApJ*, 363, 154
- Bohlin, R. C. & Savage, B. D., 1981, *ApJ*, 249, 109
- Clayton, G., Green, J., Wolff, M., Zellner, N., Code, A., & Davidsen, A. 1996, *ApJ*, (in press)
- Fitzpatrick, E. L., 1985, *ApJ*, 299, 219
- Fitzpatrick, E. L. & Savage, B. D., 1984, *ApJ*, 279, 578
- Hutchings, J. B., 1982, *ApJ*, 255, 70
- Greason, M. R., Offenber, J. D., Cornett, R. H., Hill, R. S., & Stecher, T. P. 1994, *PASP*, 106, 1151
- Hill, J. K., Bohlin, R. C., & Stecher, T. P. 1984, *ApJ*, 277, 542
- Hill, J. K., Bohlin, R. C., Cheng, K.-P., Hintzen, P. M. N., Landsman, W. R., Neff, S. G., O'Connell, R. W., Roberts, M. S., Smith, A. M., Smith, E. P., & Stecher, T. P. 1992, *ApJ*, 395, L37
- Hill, J. K., Isensee, J. E., Cornett, R. H., Bohlin, R. C., O'Connell, R. W., Roberts, M. S., Smith, A. M., & Stecher, T. P. 1994, *ApJ*, 425, 122
- Hill, J. K., et al. 1995, *ApJ*, 438, 181
- Kuno, N., Nakai, N., Handa, T., & Sofue, Y. 1995, *PASJ*, 47, 745

- Kurucz, R. L. 1992 in *The Stellar Populations of Galaxies*, ed. B. Barbuy & A. Renzini (Dordrecht: Kluwer), 225
- Lester, D. F., Harvey, P. M., & Joy, M. 1986, *ApJ*, 302, 280
- McCall M. L., Rybski, P. M., & Shields, G. A. 1985, *ApJS*, 57, 1
- Nakai, N. & Kuno, N. 1995, *PASJ*, 47, 761
- Rand, R. J. 1992, *AJ*, 103, 815
- Savage, B. D. & Mathis, J. S. 1979, *ARA&A*, 17, 73
- Schaller, G, Schaerer, D., Meynet, G., & Maeder, A. 1992, *A&AS*, 96, 269
- Schweizer, F. 1976, *ApJS*, 31, 313
- Stetson, P. B., 1987, *PASP*, 99, 101
- Stecher, T. P., et al. 1992, *ApJ*, 395, L1
- van der Hulst, J. M., Kennicutt, R. C., Crane, P. C., & Rots, A. H. 1988, *A&A*, 195, 38
- Vila-Costas, M. B. & Edmunds, M. G. 1992, *MNRAS*, 259, 121
- Waller, W. H. 1990, *PASP*, 102, 1217

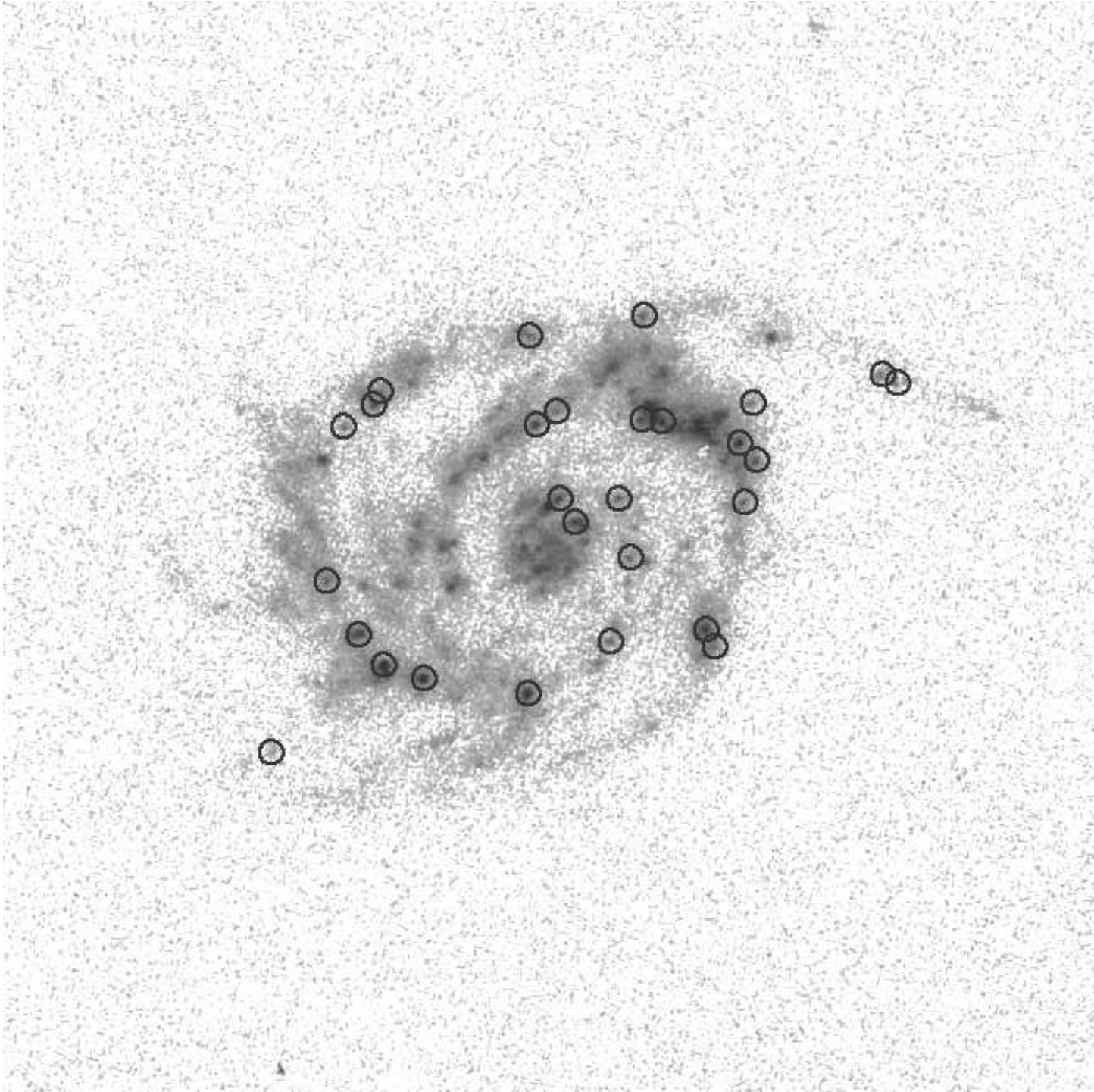


Fig. 1a.— Far-UV UIT B1 band image FUV2545 of M51. North is up, east is to the left. The 28 H II regions discussed are circled.

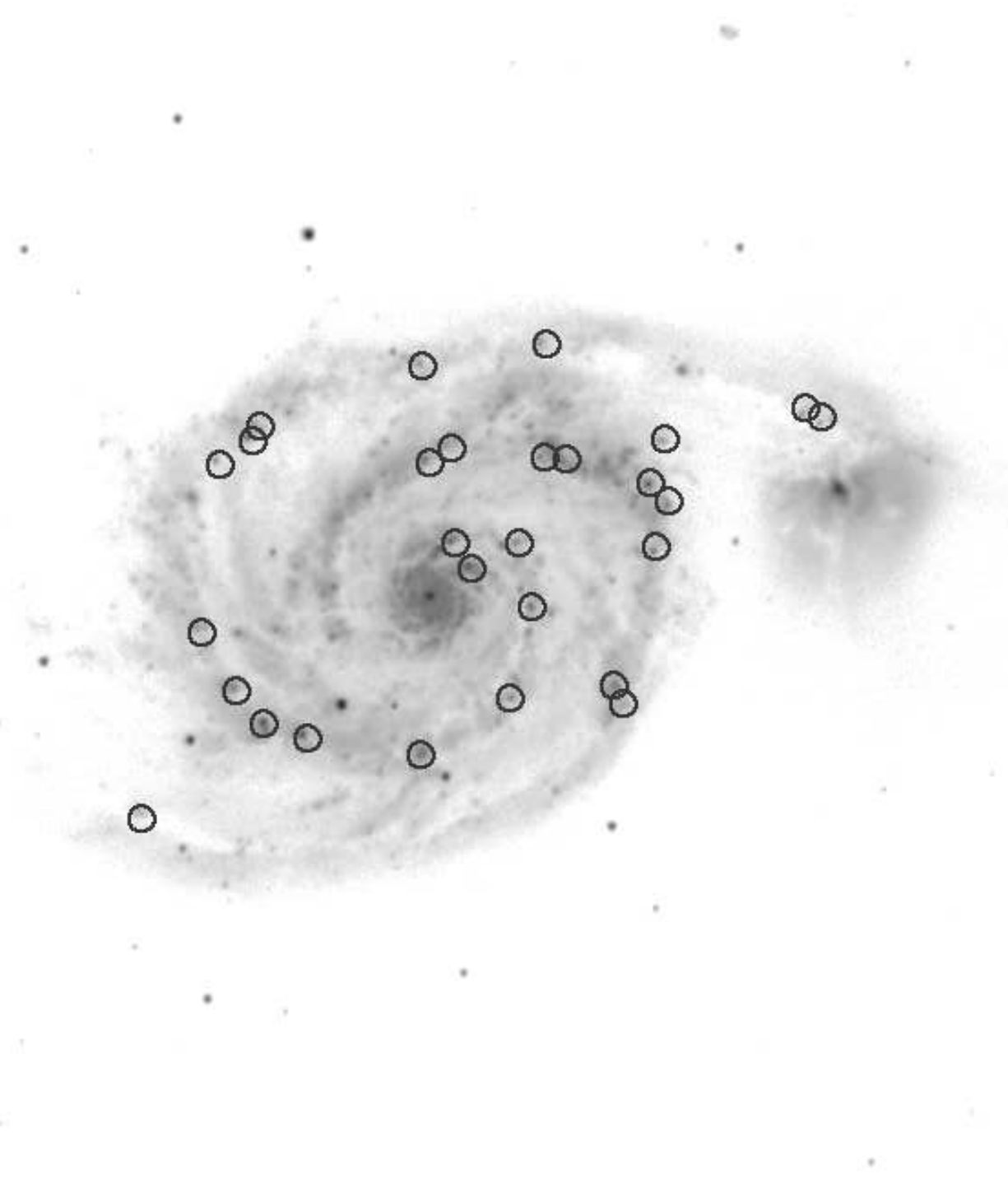


Fig. 1b.— Near-UV UIT U band image of M51, registered with Fig. 1a. The 28 HII regions discussed are circled.

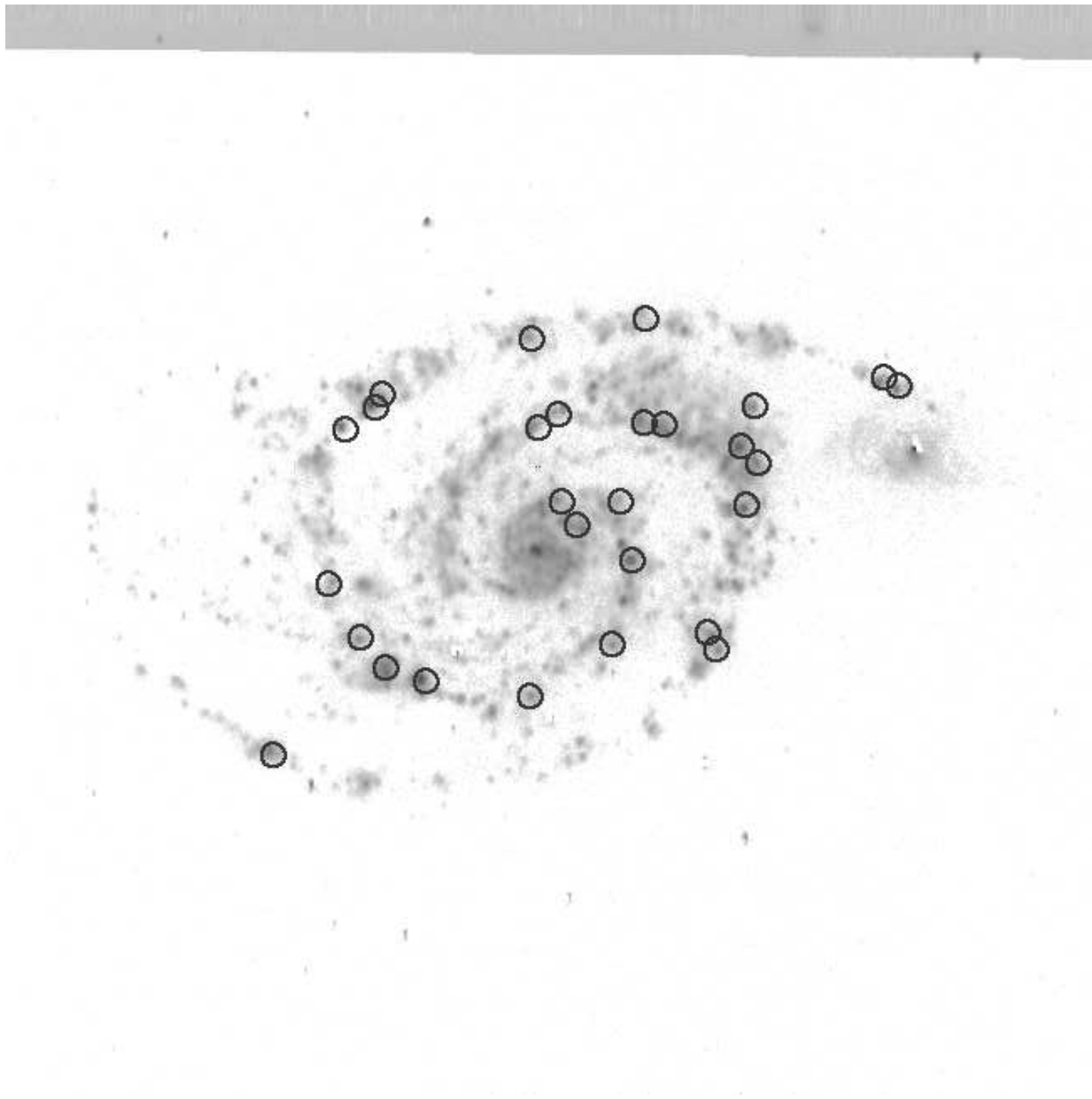


Fig. 1c.— Continuum-subtracted $H\alpha$ image of M51, registered with Fig. 1a. The 28 HII regions discussed are circled.

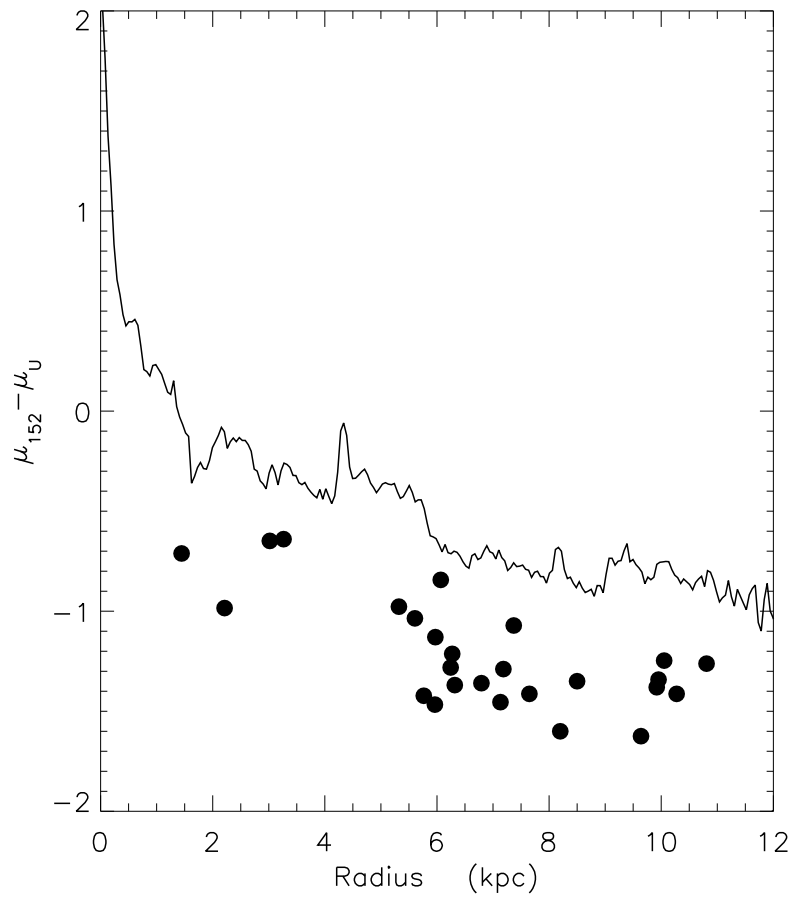


Fig. 2.— M51 $\mu_{152} - \mu_U$ radial profile. The 28 UV sources are plotted as solid circles.

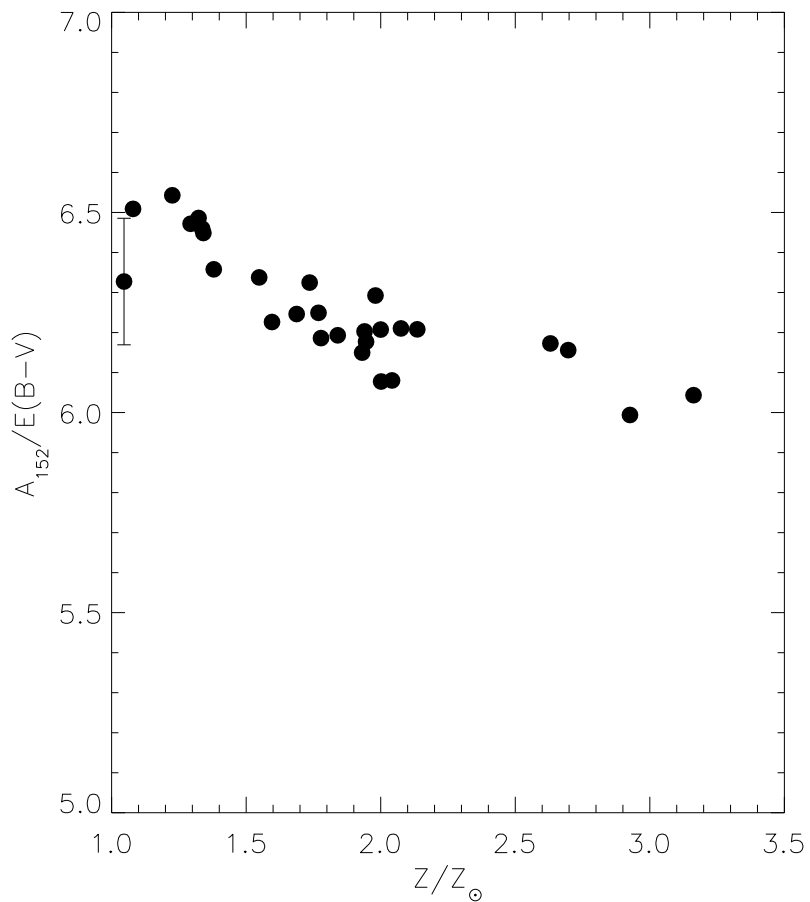


Fig. 3.— The normalized far-UV extinction $A_{152}/E(B-V)$ plotted against the metallicity Z relative to the solar metallicity. The largest metallicities occur at the smallest galactocentric radii.

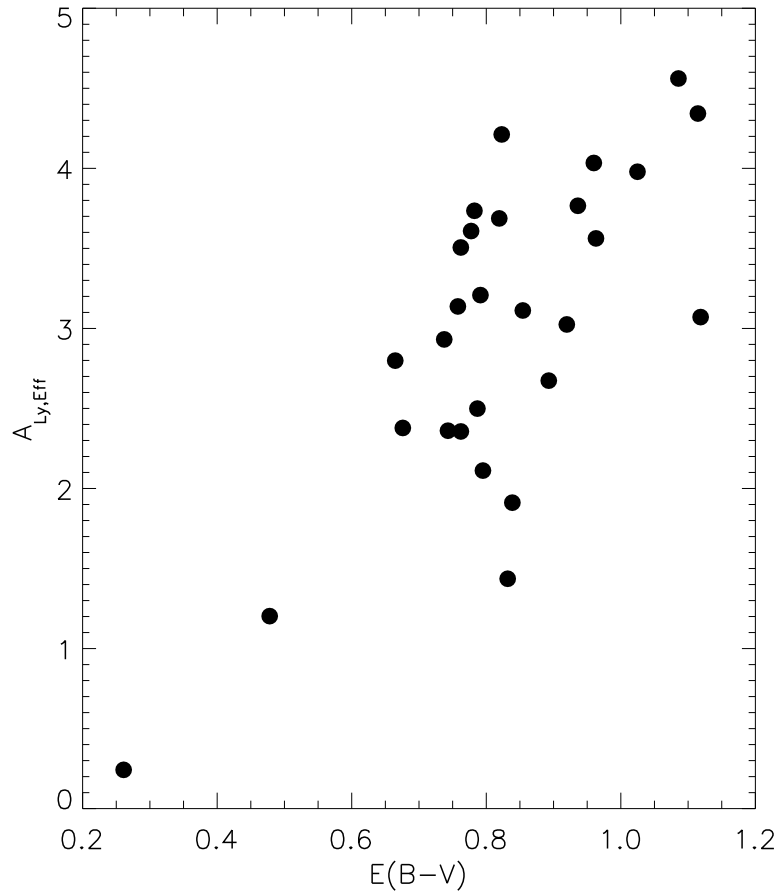


Fig. 4.— The effective Lyman continuum extinction, computed as described in the text, is plotted vs. $E(B-V)$ fit from $m_{152} - U$.